Electronic Supplementary Material (ESI) for Physical Chemistry Chemical Physics.
This journal is © the Owner Societies 2022

Supplementary Information: Metal-Water Covalency in the Photo-Aquated Ferrocyanide Complex as Seen by Multi-Edge Picossecond X-ray Absorption

Vinícius Vaz da Cruz,[1,*] Eric J. Mascarenhas,[1,2,†] Robby Büchner,[1,2] Raphael M. Jay,[2,‡] Mattis Fondell,[1] Sebastian Eckert,[1] and Alexander Föhlisch[1,2]

[1] *Helmholtz-Zentrum Berlin für Materialien und Energie GmbH, Institute for Methods and Instrumentation for Synchrotron Radiation Research, 12489 Berlin, Germany.*
[2] *Universität Potsdam, Institut für Physik und Astronomie, 14476 Potsdam, Germany.*

DETAILS OF THE MOLECULAR DYNAMICS SIMULATIONS

Initially, a cubic box of 3.4 nm length filled with water molecules was generated using the *gmx_solvate* tool from the Gromacs package [1]. All calculations used periodic boundary conditions. The temperature was controlled via a modified Berendsen thermostat (0.1 ps time constant). In the NPT runs the Parrinello-Rahman pressure-coupling was used with a 2 ps time constant. The Coulomb and van der Waals term was computed using a cut-off of 1.4 nm, while long-range electrostatics were treated via the particle mesh Ewald (PME) procedure. The energy of the initially generated system was minimized and subsequently the box was equilibrated in two steps: First, an NVT equilibration at T = 298 K was run for 500 ps (Δt = 0.5 fs), followed by an NPT equilibration at T = 298 K and P = 1 bar, which was also run for 500 ps (Δt = 0.5 fs). Lastly, a final production NPT run of 10 ns (Δt = 0.5 fs, T = 298 K and P = 1 bar) was performed from which snapshots were collected every 1 ps. This production MD run was used for extracting the snapshots for the O K-edge XAS calculations described in the main article. The radial distribution functions obtained is shown in Fig. 1, displaying the threshold used for generating the water clusters for the spectral simulations.

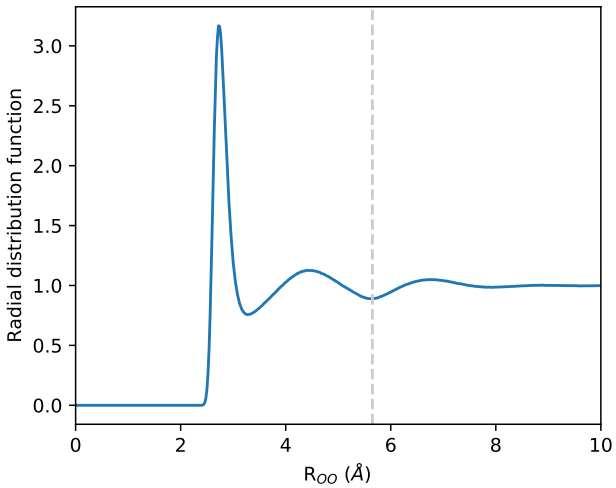

Figure 1: Oxygen-oxygen radial distribution function computed for the production run. The dashed line shows the threshhold used for generating reduced clusters for the spectral simululations discussed in the main text.

*Electronic address: vinicius.vaz_da_cruz@helmholtz-berlin.de
†Electronic address: eric.mascarenhas@helmholtz-berlin.de
‡Current address: Department of Physics and Astronomy, Uppsala University, Box 516, SE-751 20 Uppsala, Sweden

PROTONATION KINETICS OF THE DISSOCIATED CN^-

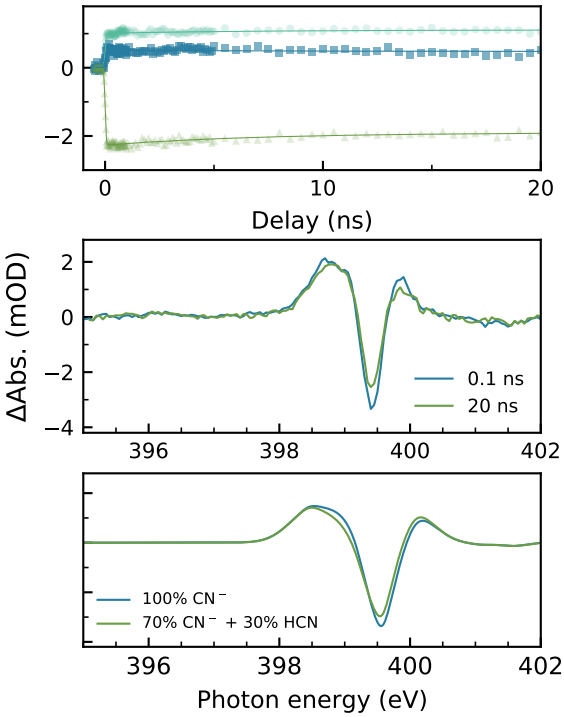

Figure 2: Protonation kinetics of the free CN^- subsequent to photoexcitation of $[Fe(CN)_6]^{4-}$ at 343 nm. A lifetime of 7 ± 1 ns for protonation of CN^- is observed.

The generated population dissociated CN^- will be protonated according to its $pK_a = 9.21$

$$CN^- + H_2O \rightarrow HCN + OH^- \tag{1}$$

this reaction was confirmed early on by pH measurements [2]. On long time-scales, We observe a weak exponential decay associated with the ground-state bleaching at the N K-edge which we believe indicates the protonation of the free cyanide ligand. From the rate model fitted to the data in the top panel of Fig. 2 we obtain a lifetime of 7 ± 1 ns for reaching the equilibrium point between CN^- and HCN. This assignment is supported by theoretical estimations that show that by decreasing the weight of free cyanide in the transient spectrum simulations from 100% to 70% and adding a 30% weight to the spectrum of HCN we obtain a decrease at the main depletion of the spectrum, in agreement with the measured data.

STATE ORDER OF THE PENTACOORDINATED SPECIES

Reinhard et al.[3] established the state order for the square-pyramidal (SP) and trigonal bipyramidal (TBP) pentacoordinated species $[Fe(CN)_5]^{3-}$ to be ^{3}TBP $<$ ^{1}SP $<$ ^{3}SP. We therefore optimized the ^{1}SP and the ^{3}TBP bond-lengths for a variety of exchange-correlation functionals restricting the bond angles between the ligands to 90° and 120°/90° (equatorial/axial), respectively. Our simulated state energies in the different geometries, summarized in Tab. I, support this order for the (range-separated) hybrid functionals. The degree of Hartree-Fock exchange in the functionals has an impact on the state order mainly destabilizing the ^{1}SP species in the case of the functionals BHANDHLYP and M062X with $\geq$50% Hartree-Fock exchange and stabilizing it for the functionals BLYP, PBE and M06L without Hartree-Fock exchange.

Table I: Simulated energies of the square-pyramidal (SP) and the trigonal-bipyramidal TBP species of $[Fe(CN)_5]^{3-}$using different exchange-correlation functionals relative to the energy of the ^{3}TBP state in eV.

Functional	^{1}SP	^{3}SP	^{1}TBP	^{3}TBP
B3LYP	0.158	0.323	0.985	0.000
PBE0	0.169	0.309	1.127	0.000
M06	0.337	0.387	1.276	0.000
WB97X	0.218	0.338	1.044	0.000
CAM-B3LYP	0.224	0.317	1.050	0.000
WB97X-V	0.150	0.336	1.017	0.000
BHANDHLYP	0.607	0.235	1.219	0.000
M062X	0.835	0.237	1.418	0.000
BLYP	-0.205	0.430	0.693	0.000
PBE	-0.322	0.444	0.724	0.000
M06L	-0.114	0.346	0.879	0.000

PSEUDO ROTATION OF $[FE(CN)_5]^{3-}$ AND WATER ATTACK

The potential energy landscape illustrated in the main article was motivated by the potential energy scans presented in Fig. 3. First, the interconversion between ^{3}SP and ^{3}TBP was assessed. Here, the bond angles in the system were restricted and the bond lengths were optimized for the different multiplicities using the B3LYP functional. The total energy of $[Fe(CN)_5]^{3-}$ in the singlet and the triplet state is presented in Fig 3a as a function of the pseudo rotation angle θ connecting the SP and the TBP structures. The curves connect the two configurations and extend the view achieved through the single point energies listed in Tab. I by showing that the crossing of the singlet and triplet curves occurs near the SP geometry.

Secondly,the water attack was investigated based on the potential energy curves along the Fe-OH_2 bond in Fig. 3b. They further illustrate that aquation of the complex is favoured in the SP geometry, as the curves of the TBP structure are highly dissociative for both multiplicities. Only the ^{1}SP curve exhibits a clearly bonding character. Here, the bond lengths were optimized for the isolated $[Fe(CN)_5]^{3-}$ species in the respective spin state. Then the Fe-OH_2 bond distance was scanned keeping all remaining degrees of freedom fixed.

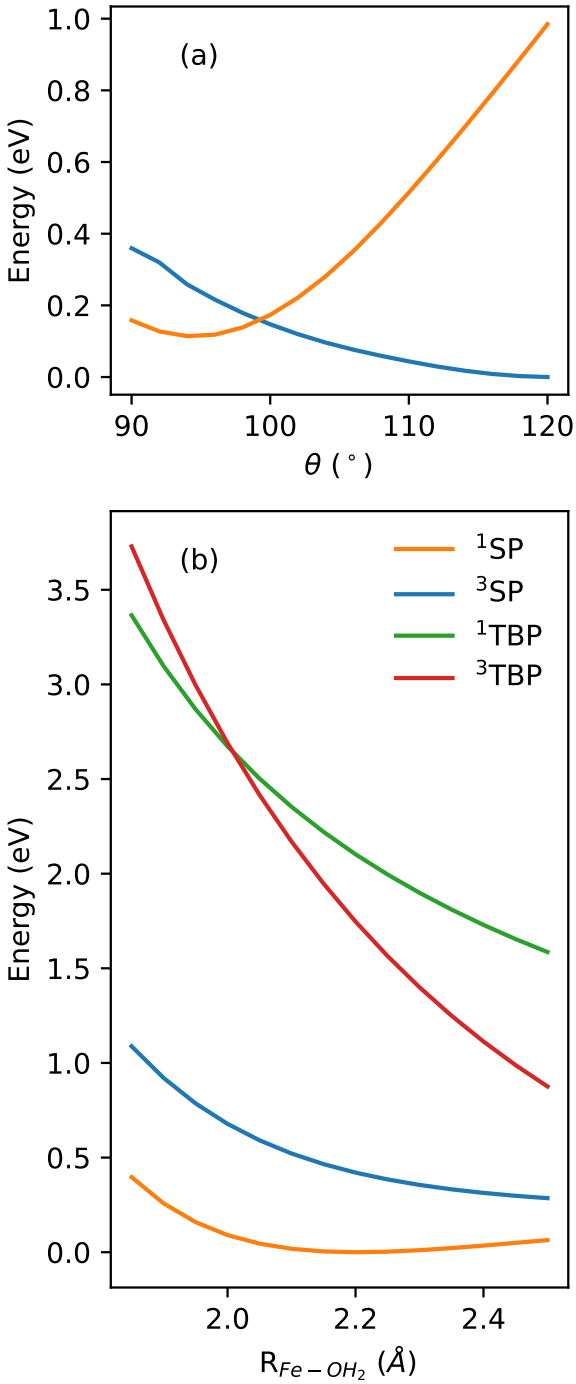

Figure 3: Pseudo rotation and attack of a water molecule on the $[Fe(CN)_5]^{3-}$ species. (a) Singlet and triplet state energies as a function of the equatorial angle θ (as defined in the main study) spanning the range between the SP ($\theta = 90°$) and the TBP geometry $\theta = 120°$. (b) Potential energy curves along the Fe-OH_2 bond for the SP and TBP structures in the singlet and triplet state.

EFFECT OF SPIN-ORBIT COUPLING ON THE SIMULATED SPECTRAL SIGNATURES AT THE FE L-EDGE

The effects of spin-orbit coupling (SOC) on the iron L-edge spectrum simulations of ground-state $[Fe(CN)_6]^{4-}$ and the transient spectrum are assessed in Fig. 4. Both TD-DFT with and without SOC provide a qualitatively correct description of the experimental spectra, the main differences associated with the intensity ratios. Particularly, the region around the main e_g resonance seems rather insensitive to SOC effects.

As mentioned in the main text, SOC calculations within the TD-DFT framework are only implemented in Orca for a singlet KS reference. Therefore, we carried out additional DFT/ROCIS calculations to assess the effect of spin-orbit coupling also for the triplet pentacoordinated intermediates discussed in the main text. A comparison to DFT/ROCIS based spectrum simulations is given in Fig 5. Overall the inclusion of spin-orbit coupling does not have a strong effect on the predicted spectral signatures. Even though quantitative differences in the simulated resonance energies and intensities are present, the qualitative spectral signatures support the TD-DFT ones included in the main text, as shown in Fig 5.

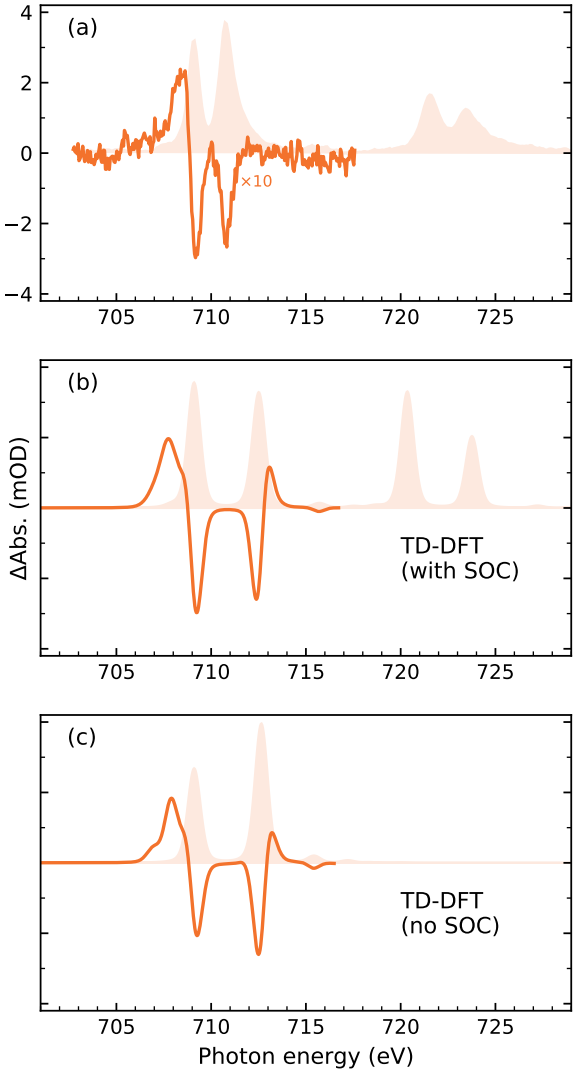

Figure 4: Effect of spin-orbit coupling on the predicted transient signatures of $[Fe(CN)_6]^{4-}$ and $[Fe(CN)_5(H_2O)]^{3-}$ in the TD-DFT spectrum simulations. Comparison of the experimental data (a), L-edge TD-DFT simulations with (b) and without (c) consideration of spin-orbit coupling effects.

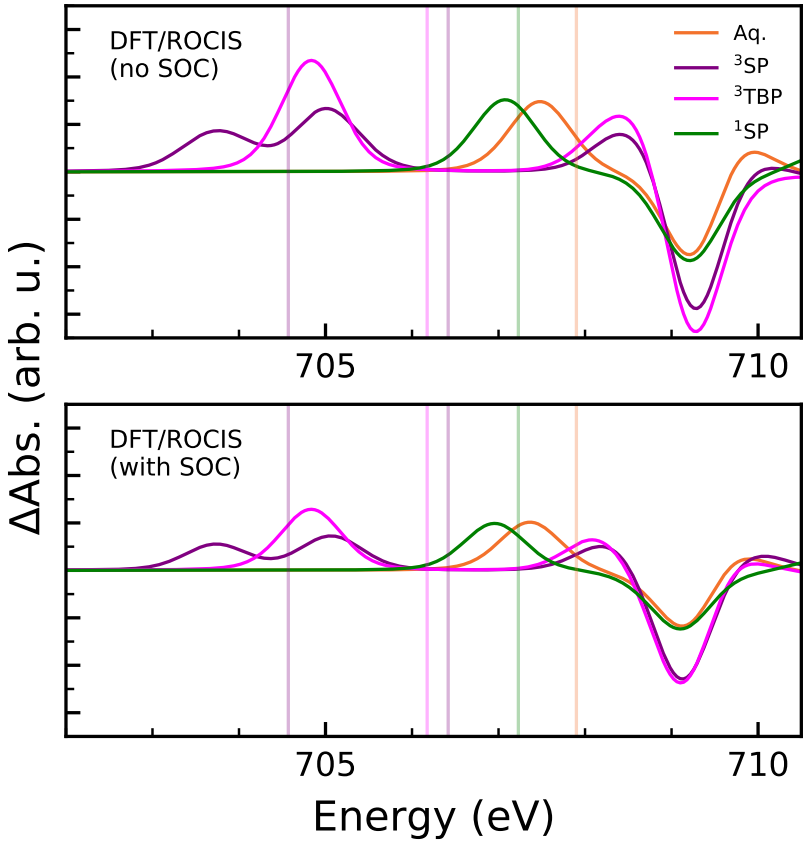

Figure 5: DFT/ROCIS simulations of L_3 spectral signatures of transient species in the photo-aquation pathway with and without considering spin-orbit coupling effects. The vertical lines indicate the TD-DFT transition energies shown in the main text.

TRANSIENT OXYGEN K-EDGE SIGNATURES

To support the assignment of the transient pre-edge feature below the water O 1s→4a$_1$ band to the covalent interaction between the coordinating water molecule and $[Fe(CN)_5]^{3-}$, we also performed additional pump-probe measurements, under equivalent conditions, on a pure water sample. In the data, presented in Fig. 6, the pre-edge feature is not existent for laser-excitation of pure water, further supporting its assignment to the $[Fe(CN)_5(H_2O)]^{3-}$ species.

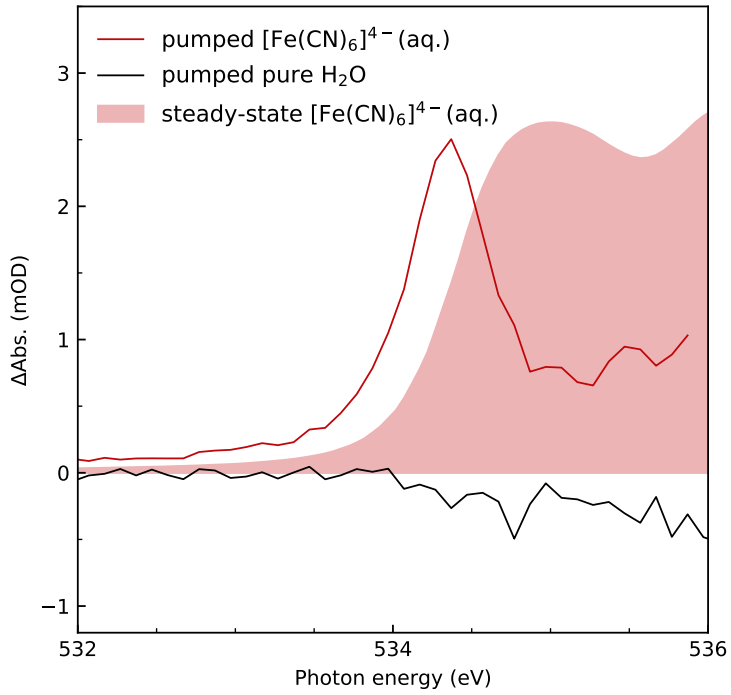

Figure 6: Robustness of the transient signature at the oxygen K-edge. Transient spectra of $[Fe(CN)_6]^{4-}$ (aq.) and pure water excited at a wavelength of 343 nm at a pump-probe delay of 100 ps.

[1] Lindahl, Abraham, Hess, and van der Spoel, Gromacs 2019 source code, URL https://doi.org/10.5281/zenodo.2424363.
[2] A. G. MacDiarmid and N. F. Hall, Journal of the American Chemical Society **75**, 5204 (1953), ISSN 0002-7863, URL https://doi.org/10.1021/ja01117a017.
[3] M. Reinhard, G. Auböck, N. A. Besley, I. P. Clark, G. M. Greetham, M. W. D. Hanson-Heine, R. Horvath, T. S. Murphy, T. J. Penfold, M. Towrie, et al., Journal of the American Chemical Society **139**, 7335 (2017), ISSN 0002-7863, URL https://doi.org/10.1021/jacs.7b02769.